MICRO-SCALE SHEET RESISTANCE MEASUREMENTS ON ULTRA SHALLOW JUNCTIONS

Christian L. Petersen[†], Rong Lin[‡], Dirch H. Petersen[‡], Peter F. Nielsen[‡]
[†]CAPRES A/S, Burnaby, BC, Canada
[‡]CAPRES A/S, Lyngby, Denmark

We report a new method for measuring sheet resistance on implanted wafers by using micro-fabricated four-point probes with a tip-to-tip spacing of a few microns. These microscopic probes have a contact force five orders of magnitude smaller than conventional probes, and can perform local non-destructive Ultra Shallow Junction (USJ) sheet resistance measurements on both blanket and patterned wafers. We demonstrate this new technique on laser annealed wafers, measuring micro-scale sheet resistance variations on wafers that appear homogeneous when mapped with conventional four-point probes. The microscopic four-point probes detect stitching effects caused by laser spot overlap/misalignment during the annealing process. Our findings indicate that such local sheet resistance inhomogeneities average out in conventional four-point measurements, and that new metrology is therefore needed to fully characterize USJ wafers activated by laser anneal and other diffusion-less methods.

INTRODUCTION

A transistor in a semiconductor circuit consists of two implanted regions, called the source and drain, connected electrically by a channel under a gate electrode. The Source Drain Extension (SDE) is a shallow implant that interfaces the channel under the gate with the deep source and drain. As transistors are made smaller, the SDE must be made extremely shallow to create a high performance device [1]. Such SDE implants are termed Ultra-Shallow Junctions (USJs).

Historically, macroscopic four-point probes have been the standard for measuring active dose in implanted wafers. A macroscopic four-point probe is a millimeter-sized device with four spring-loaded transition metal needles in a single row. When the needles press against a surface, a current driven through the outer two pins generates a detectable voltage across the inner pins. This four-point measurement technique has been used to measure sheet resistance on semiconductors for many years [2].

However, macroscopic four-point probes perform poorly on USJ, as the spring-loaded needles tend to create surface damage and film penetration [3]. The macroscopic probes also require large homogenous areas for measurements without edge artifacts, making it necessary to measure sheet resistance on expensive sacrificial wafers.

Several new technologies attempt to improve this conventional sheet resistance metrology, including macroscopic probes with low contact force [4] and capacitive non-contact probes [5]. While addressing the penetration issue, these new probes are even larger than the conventional four-point probes.

This paper introduces an alternative technology, microscopic four-point probes [6, 7]. These probes are very small, non-destructive, and rely on the same principle as the conventional probes. In this way they offer a simple and straightforward solution to both size and penetration issues of conventional sheet resistance metrology.

MICROSCOPIC FOUR-POINT PROBES

The microscopic four-point probes are silicon-based MEMS devices with arrays of micron-scale cantilever electrodes, as shown in Fig. 1. The cantilevers extend from the edge of a probe support, and consist of SiO_2 with a thin metallic coating [7]. The cantilevers are typically 10 - 30 μm long and 500 nm - 2 μm wide. The smallest tip-to-tip

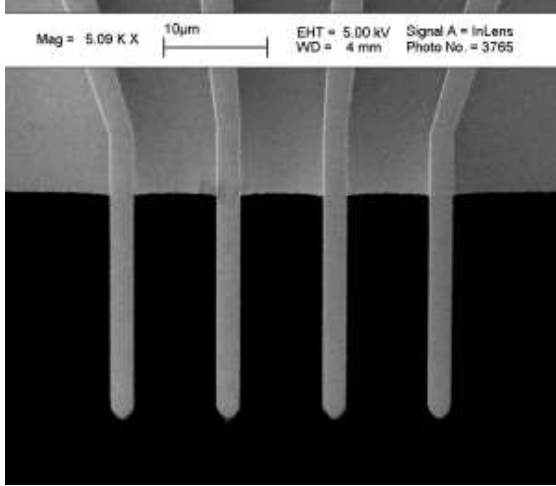Figure 1: Scanning Electron Microscope (SEM) image of a microscopic four-point probe. The cantilever electrodes are 2 μm wide and 25 μm long. The tip-to-tip spacing spacing is 10 μm, 100$\times$ smaller than that of a conventional probe.

Figure 2: Schematic of four-point probe measurements on an implanted semiconductor surface as a function of probe electrode spacing.

spacing achieved with this technology is currently 1 μm. Several types of these probes with different electrode spacing and properties are commercially available [8].

The use of MEMS processing makes geometric variations minimal. This is in contrast to the conventional four-point probes where such variations make probe to probe calibrations necessary.

The microscopic four-point probes need more elaborate electrical and mechanical interfacing than conventional probes. For example, the typical current set-point is 10-50μA, several orders of magnitudes smaller than before. A high-precision current source and a high-impedance electrometer must therefore be in close proximity to the probe in order to minimize electrical noise.

The mechanical stability and resolution of the measurement system is also important. Submicron resolution is needed to ensure repeatable results, as well as to allow the probe cantilevers to touch down onto a sample without damage to the surface. The contact force is determined by the cantilever deflection, and is typically five to six orders of magnitude smaller than that of a conventional probe. In fact, the probe cantilevers form an elastic contact to the sample surface, and electrical contact is established through the native oxide
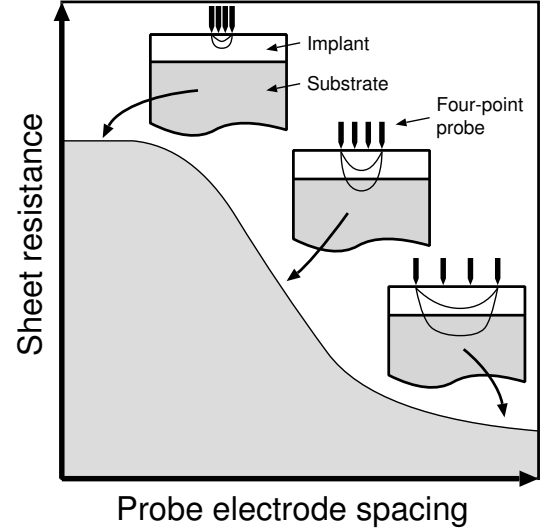
by an electrical breakdown mechanism.

PROBING LENGTH SCALE

One of the benefits of using a microscopic four-point probe is the increased surface sensitivity, as illustrated schematically in Fig. 2 for an implanted sample. It is intuitively clear that a measurement performed with a limiting small electrode spacing will reflect only transport in the implanted layer, irrespective of the substrate condition. On the other hand, a measurement performed with large electrode spacing will represent the parallel combination of the implant and the substrate. The transition electrode spacing separating these two regimes depends on the resistance area product of the interface in between implant and substrate as well as the sheet resistance of the two regions. In a simple model of two semi-infinite sheets this transition electrode spacing is given by [9]

$$\lambda = \sqrt{\frac{RA}{R_{implant} + R_{substrate}}}, \qquad (1)$$

where RA is the resistance area product of the interface, $R_{implant}$ is the implant sheet resistance and $R_{substrate}$ is the substrate sheet resistance.
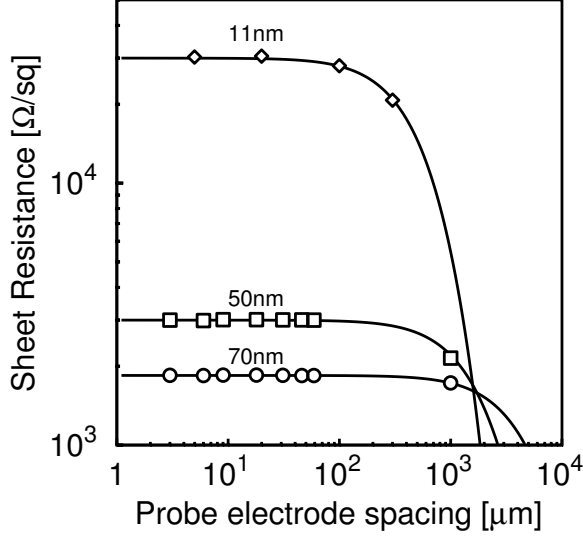
Figure 3: Four-point measurements as a function of electrode spacing on 11 nm, 50 nm and 70 nm deep profiles.

Figure 4: Ratio of measured sheet resistance to actual sheet resistance for probes with electrode spacing 10 μm, 100 μm, 1 mm and 2 mm, as function of junction leakage current density.

$R_{substrate}$ is related to the substrate resistivity ρ through $R_{substrate} = \rho/t$, where t is the thickness of the substrate.

In the case of Ultra Shallow Junctions, the interface is effectively a diode type barrier with a strongly non-linear behavior. The current density through the barrier can be expressed

$$J = J_s(e^{qV/kT} - 1), \qquad (2)$$

where V is the potential across the interface and J_s the saturation current density. If the potential across the interface is much smaller than the thermal voltage at 300 K, kT/q = 25.9 mV, this expression reduces to

$$J = \frac{VJ_sq}{kT}. \qquad (3)$$

This is a valid approximation on USJ implants when measurements are performed at a current set-point of a few μA, leading to a potential drop on the order of a few mV between the inner electrodes (since typical USJ sheet resistance lies in a narrow range of 500 - 2000 Ω/sq). The potential across the barrier will only be a fraction of this inner electrode potential. In this regime, the resistance-area product RA for the barrier is
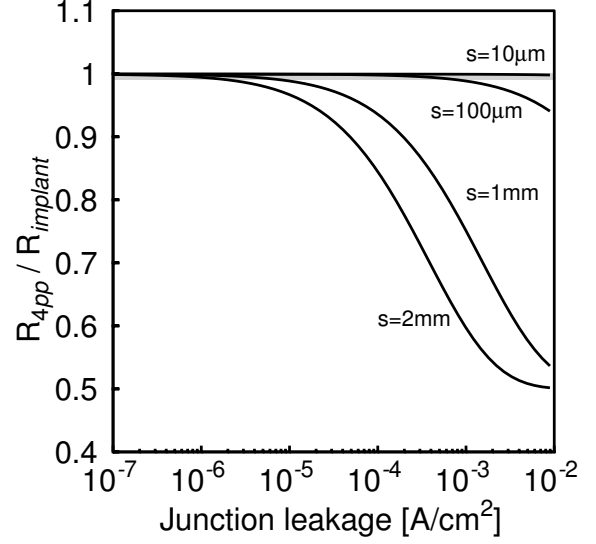
$$RA = \frac{kT}{J_sq}. \qquad (4)$$

Typical leakage current densities are in the range of 10^{-7} to 10^{-3} A/cm^2. Inserting values in Eq. 4 and Eq. 1 then shows that USJ samples have a transition probe electrode spacing on the order of millimeters. Higher leakage current lead to smaller transition electrode spacing. High leakage current densities are common in USJ samples annealed by diffusion-less technologies such as laser anneal, and in samples with high substrate doping (either bulk or halo).

Fig. 3 shows measurements on three semiconductor samples with profiles of 11 nm (diamond bullets), 50 nm (square bullets) and 70 nm (circle bullets) respectively. The microscopic four-point probe measurements were performed using micro-fabricated probes at probe spacing ranging from 3 to 300 μm. The macroscopic measurement was performed with a conventional needle probe. The current set-point was 50 μA. For all three samples, the measured sheet resistance forms a plateau at the smallest electrode spacing, and drops significantly at larger electrode spacing. This is as expected from Fig. 2.

In the semi-infinite sheet approximation considered here, the measured sheet resistance of a

probe with spacing s is given by

$$R_{4pp} = \frac{R_{implant}R_{substrate}}{R_{implant} + R_{substrate}}\frac{1}{2\pi} \times \quad (5)$$
$$(\frac{2R_{implant}}{R_{substrate}}(K_0(\frac{s}{\lambda}) - K_0(\frac{2s}{\lambda})) +$$
$$\log 4),$$

where K_0 is the modified Bessel function of the second kind of order zero.

The substrate sheet resistance was $R_{substrate}$ = 15 Ω/sq. A fit of the data in Fig. 3 to Eq. 5 then leads to $R_{implant}$ = 30.3$\times 10^3$ Ω/sq and λ = 0.55 mm for the 11 nm sample, $R_{implant}$ = 3006 Ω/sq and λ = 1.92 mm for the 50 nm sample and $R_{implant}$ = 1847 Ω/sq and λ = 5.66 mm for the 70 nm sample. The fitted theoretical predictions are shown as solid lines in Fig. 3.

Eq. 4 and Eq. 5 can be used to calculate the deviation in measured sheet resistance for different probe spacing as a function of junction leakage. This is illustrated in Fig. 4 for $R_{implant}$ = $R_{substrate}$ = 1000 Ω/sq. The figure shows the ratio of measured sheet resistance to actual sheet resistance. It is clear that a conventional millimeter sized four-point probe measures significantly lower than the actual value at current leakage densities above 10^{-5} A/cm^2. On the other hand, a microscopic probe with 10μm spacing is seen to remain accurate in the entire range considered.

MICROSCOPIC MAPPING

The closely spaced pins of the microscopic four-point probe make it possible to image sheet resistance at high resolution. This enables detection of local features that average out when conventional large probes are used. An example of such micro-scale features is shown in Fig. 5. This figure shows local sheet resistance measurements in an implanted wafer activated by laser anneal. The periodic sheet resistance variations are due to a laser spot stitching effect. The periodic variations, although dramatic, are invisible in a conventional four-point probe wafer map.

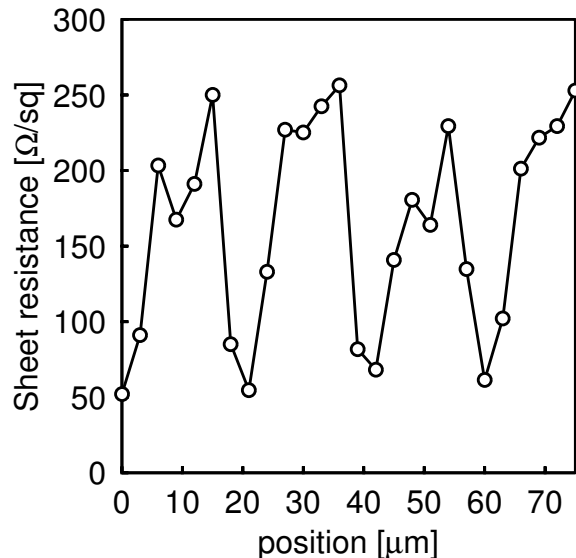The measurement in Fig. 5 has a period of about 20 μm. Many other laser annealed samples

Figure 5: Micro-scale sheet resistance line scan on a laser annealed implanted wafer. The probe spacing was 3.0 μm.

have been measured, and they all exhibit micro-scale features. The period varies depending on the particularities of the different laser anneal tools used. Similar micro-scale sheet resistance variations are likely to be present in other types of advanced USJ activation methods as well, due to interference and pattern effects.

It is critically important to control these micro-scale sheet resistance artifacts, and metrology is needed to visualize them. Micro-scale four-point probes offer a straightforward solution.

SHEET RESISTANCE ON PRODUCT WAFERS

Blanket test wafers are an increasing problem in semiconductor manufacturing as the wafers are becoming prohibitively expensive. Blanket wafers for four-point probe testing in the implant/anneal cycle alone already costs semiconductor fabs millions of dollars per year.

Microscopic four-point probes make it possible to measure sheet resistance on product wafers. A four-point probe needs a homogenous surface area much wider than the probe spacing in order
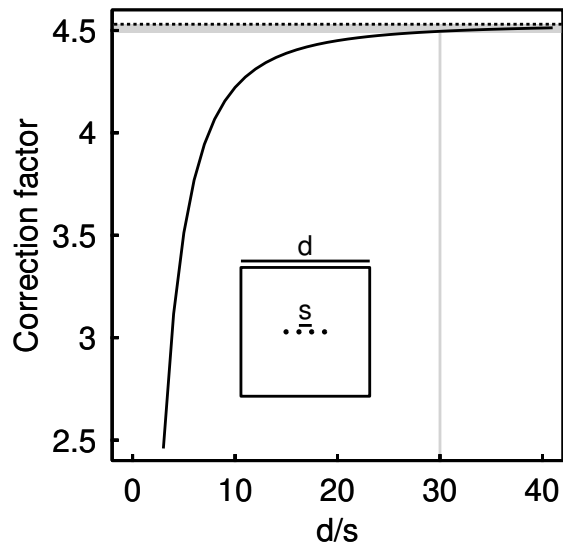
Figure 6: The four-point probe geometric correction factor as function of the ratio between sample width d and electrode spacing s for a probe centered on a square sample. The dotted line represents the limit of an infinite sheet ($d \to \infty$).

to make a measurement without geometry artifacts. This is illustrated in Fig. 6. The geometric error is less than 1% only when the ratio of spacing to sample width is larger than 30. This means that a conventional four-point probe needs an area at least 3 cm wide in order to make good measurements. On the other hand, a microscopic probe with 1 μm spacing is able to make an accurate measurement in a area of just 30 μm in width. It is thus possible to perform accurate measurements in a box the size of a typical bonding pad, and sheet resistance probing can be moved from blanket wafers to product wafer scribe lines or test dies.

In addition to eliminating test wafers, moving sheet resistance metrology onto the product wafers can improve measurement accuracy and thus potentially improve process control and qualification.

CONCLUSION

We have demonstrated how microscopic four-point probes can improve conventional sheet resistance metrology on USJ.

The microscopic probes do not penetrate the extremely thin junctions, and the small electrode spacing ensures that the measurements reflect only transport in the implanted layer, irrespective of the substrate doping and junction leakage. Conventional four-point probes have been shown to measure values that are too low if the junction leakage is high. This effect is present even when no penetration occur. High junction leakage is known to appear when activation is done by diffusion-less methods such as laser anneal.

We have shown how microscopic four-point probes can be used to resolve local sheet resistance variations which average out in conventional four-point probing. This is of particular importance where local variations appear due to inhomogeneous annealing processes.

Finally, we have shown how it is possible to make accurate sheet resistance measurements without geometric corrections using microscopic four-point probes centered in boxes as small as 30 μm square. This makes it possible for the first time to perform true sheet resistance measurements on product wafers. In this way, microscopic four-point probes offer a powerful method for USJ sheet resistance characterization, that address all of the shortcomings of the conventional technology.

The authors thank Wilfried Vandervorst and Trudo Clarysse from IMEC for provision of samples.

REFERENCES

[1] "International technology roadmap for semiconductors." [Online]. Available: www.itrs.net

[2] F. M. Smits, *Bell Sys. Tech. J.*, vol. 37, p. 711, 1958.

[3] T. Clarysse, A. Moussa, F. Leys, R. Loo, W. Vandervorst, B. M. C., R. J. Hillard, V. N. Faifer, M. I. Current, R. Lin, and D. H. Petersen, *Mat. Res. Soc. Proc.*, vol. 912, p. C5.7, 2006.

[4] R. J. Hillard, R. G. Mazur, W. J. Alexander, C. Win Ye, M. C. Benjamin, and J. O. Bor-

land, *Mat. Res. Soc. Proc.*, vol. 810, p. C11.6, 2004.

[5] V. N. Faifer, M. I. Current, T. M. H. Wong, and V. V. Souchkov, *J. Vac. Sci. Technol. B*, vol. 24, p. 414, 2006.

[6] C. L. Petersen, F. Grey, I. Shiraki, and S. Hasegawa, *Appl. Phys. Lett.*, vol. 77, p. 3782, 2000.

[7] C. L. Petersen, T. M. Hansen, P. Bøggild, A. Boisen, O. Hansen, T. Hassenkam, and F. Grey, *Sensors and Actuators A*, vol. 96, p. 53, 2002.

[8] [Online]. Available: www.capres.com

[9] D. C. Worledge and P. L. Trouilloud, *Appl. Phys. Lett.*, vol. 83, p. 84, 2003.